

Electron capture in collisions of N^+ with H and H^+ with N

C. Y. Lin* and P. C. Stancil†

*Department of Physics and Astronomy and the Center for Simulation Physics
The University of Georgia, Athens, GA, 30602-2451*

J. P. Gu and R. J. Buenker‡

*Fachbereich C-Mathematik und Naturwissenschaften,
Bergische Universität Wuppertal, D-42097 Wuppertal, Germany*

M. Kimura§

Graduate School of Sciences, Kyushu University, Fukuoka 812-8581, Japan

(Dated: March 8, 2005)

Abstract

Charge transfer processes due to collisions of N^+ with atomic hydrogen and H^+ with atomic nitrogen are investigated using the quantum-mechanical molecular-orbital close-coupling (MOCC) method. The MOCC calculations utilize *ab initio* adiabatic potentials and nonadiabatic radial and rotational couplings obtained with the multireference single- and double-excitation configuration interaction approach. Total and state-selective cross sections for the energy range 0.1 meV/u - 1 keV/u are presented and compared with existing experimental and theoretical data. A large number of low-energy resonances are obtained for exoergic channels and near thresholds of endoergic channels. Rate coefficients are also obtained and comparison to previous calculations suggests nonadiabatic effects dominate for temperatures greater than 20,000 K, but that the spin-orbit interaction plays a major role for lower temperatures.

PACS numbers: 34.10.+x, 34.20.Mq, 34.70.+e

*Electronic address: cylin@hal.physast.uga.edu

†Electronic address: stancil@physast.uga.edu

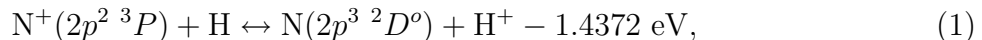
‡Electronic address: buenker@uni-wuppertal.de

§Electronic address: mineoscc@mbx.nc.kyushu-u.ac.jp

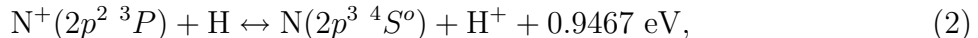
I. INTRODUCTION

In the electron capture process electrons are transferred from one atomic system to another during a collision. The importance of electron capture is not only in understanding of dynamical mechanisms for atomic and molecular collisions, but also in practical applications. In many environments of current research, such as planetary atmospheres and astrophysical and laboratory plasmas, charge transfer can have a crucial influence. Because of the abundance of ions in astronomical environments, charge transfer may be the dominant process in establishing the ionization balance and may also influence spectral line emission. In addition, a deeper understanding of the electron capture process will also help in modeling the edge region of tokamak fusion plasmas [1].

In this work we investigate the reactions



and



using the quantum-mechanical molecular-orbital close-coupling (MOCC) method. A brief description of the theoretical methods is presented in section II. In section III, the adiabatic potentials and nonadiabatic couplings of NH^+ are discussed. The resulting cross sections and rate coefficients including total and state-selective are given in section IV and compared with the existing experimental data and previous calculations. Section V gives a summary of the work. Atomic units are used unless otherwise noted.

II. THEORETICAL METHODS

A. Electronic Structure Calculations

The *ab initio* adiabatic potentials and nonadiabatic couplings in the present work are obtained from the multireference single- and double-excitation configuration interaction (MRD-CI) method which has been detailed earlier in Buenker and coworker's publications [2–4]. Here only information relevant to the present calculation is specified. The atomic orbital basis sets for molecular calculations consist of contracted Gaussian functions. The $(8s2p)$ basis for the hydrogen atom is contracted in $[5s2p]$ and augmented by one *s*-, one *p*- and

one d -type diffuse function with exponents which are 0.0195, 0.042 and 1.1 respectively. For the nitrogen atom, the $(15s10p2d)$ basis is contracted in $[9s6p2d]$. Eight molecular states including five doublets and three quartets are considered for collisions of the NH^+ system. The finite difference technique [5, 6] has been applied to obtain radial couplings (matrix elements of $\partial/\partial R$), while rotational couplings have been calculated by employing appropriate pairs of CI eigenfunctions.

B. Scattering Theory

The quantum-mechanical MOCC approach, which has been described in the literatures [7, 8], is used in the present calculation. Only a brief outline is given here. For the nonrelativistic Hamiltonian of the NH^+ system with the total wave function expanded in products of molecular electronic and nuclear wave functions, we use the perturbed stationary state approximation to find the scattering solutions. Carrying out the variation of the set of nuclear wave functions, we obtain a set of second-order coupled equations in the adiabatic representation. Although we may solve the equations in the adiabatic representation, it is numerically more convenient to make a unitary transformation which converts the coupled equations into a diabatic representation. A coupled set of second-order differential scattering equations without first-order derivatives can then be solved by using the multichannel log-derivative method of Johnson [9]. From the numerical results and the analytical asymptotic expressions of the radial functions, the K -matrix may be extracted and thus the S -matrix is given by

$$S_J = \frac{I + iK_J}{I - iK_J} \quad (3)$$

where J is the total angular momentum and I is the identity matrix. The charge transfer cross sections from the channel α to the channel β are expressed in terms of the scattering matrix elements

$$\sigma_{\alpha \rightarrow \beta} = \frac{\pi g_\alpha}{k_\alpha^2} \sum_J (2J + 1) |S_J|_{\alpha\beta}^2, \quad (4)$$

where k_α denotes the wave number for the center-of-mass motion of the initial incoming channel and g_α is the initial approach probability factor.

III. POTENTIALS AND COUPLINGS

For the present calculations, adiabatic potentials for NH^+ include eight molecular states which are $1^4\Sigma^-$, $2^4\Sigma^-$, $1^4\Pi$, $1^2\Sigma^-$, $2^2\Sigma^-$, $1^2\Pi$, $2^2\Pi$ and $1^2\Delta$. Fig. 1 shows the adiabatic potentials as a function of internuclear distance R for $R = 1$ to 10 (a.u.). As internuclear distance approaches infinity, these eight molecular states will degenerate into three separated-atom states which are $\text{N}(2p^3^4S^o)+\text{H}^+$, $\text{N}^+(2p^2^3P)+\text{H}$ and $\text{N}(2p^3^2D^o)+\text{H}^+$. The corresponding relations are displayed in table 1.

The interactions between different molecular states result from nonadiabatic radial and rotational couplings. Radial coupling results from the interaction between molecular states of the same symmetry ($\Lambda=\Lambda'$) while rotational coupling is due to interaction between molecular states of different symmetry ($\Lambda=\Lambda'\pm 1$), where Λ is the projection quantum number of the electronic orbital angular momentum onto the internuclear axis. Nonadiabatic couplings as a function of R are plotted in Fig. 2. The radial couplings include interactions of two quartet Σ^- states, two doublet Σ^- states, and two doublet Π states, while the rotational couplings comprise interactions of the quartet Π state with quartet Σ^- states, and doublet Π states with doublet Σ^- and Δ states.

Given adiabatic potentials and couplings, we transform them to a diabatic representation by a unitary transformation [10]. In Fig. 3, several diagonal diabatic potentials are plotted and compared with the adiabatic potential energies. It is clear that the adiabatic potential curves of the same symmetry don't cross, but crossings may occur in the diabatic representation. However, adiabatic and diabatic potential curves will merge into identical asymptotical atomic energies at large R . In order to get reliable cross sections near the threshold, we make an asymptotic fit to join the *ab initio* data smoothly to the long range form $-\frac{\alpha}{2R^4}$, where α is the dipole polarizability. We adopted $\alpha = 4.50$ for H and $\alpha = 7.42$ and 11.17 for $\text{N}(2p^3^4S^o)$ and $\text{N}(2p^3^2D^o)$ respectively.

Several major off-diagonal diabatic couplings are illustrated in Fig. 4. The couplings in Fig. 4a show the important interactions between the asymptotic atomic states of $\text{N}(2p^3^4S^o) + \text{H}^+$ and $\text{N}^+(2p^2^3P) + \text{H}$ for the charge transfer process in the NH^+ system, while the couplings in Fig. 4b give us the important interactions between $\text{N}^+(2p^2^3P) + \text{H}$ and $\text{N}(2p^3^2D^o) + \text{H}^+$. The related adiabatic labelings corresponding to a specific diabatic coupling are indicated above the symbol in the figures.

IV. RESULTS AND DISCUSSION

A. Cross Sections

The state-selective cross sections for the electron capture process are evaluated by using the molecular electronic structure and coupling data in Sec. II, but with the potentials shifted to match the experimental asymptotic energies as listed in Table I. The contributions from the individual partial waves are summed as in Eq. (4) until a convergence of the state-selective cross section is achieved. The total cross section then can be obtained from the sum of state-selective cross sections. The results over the energy range from 0.1 meV/u to 1 keV/u are illustrated in Fig. 5 for total cross sections and state-selective cross sections of reactions (1) and (2), which are endoergic and exoergic respectively. In our calculation, reaction (1) includes five channels, $1\ ^2\Sigma^-$, $1\ ^2\Pi$, $2\ ^2\Sigma^-$, $2\ ^2\Pi$ and $2\ ^2\Delta$, while there are three channels including $1\ ^4\Sigma^-$, $1\ ^4\Pi$ and $2\ ^4\Sigma^-$ in reaction (2). It is clear from the cross sections that for the energy region between 10 and 500 eV/u capture into $N(2p^3\ ^4S^o)$ is the dominant path. As the collision energy approaches 1.53 eV/u, cross sections for capture into the $N(2p^3\ ^2D^o)$ decrease rapidly to zero because of the approach of the $N(2p^3\ ^2D^o) + H^+$ threshold. In addition, from the inset plot of Fig. 5, we find several orbiting resonances [1] due to quasibound rovibrational states of the quasimolecule. Although these features have been found and studied theoretically in different collision systems [11], there is still no experimental verification. On the other hand, cross sections for capture into the $N(2p^3\ ^4S^o)$ display Langevin behavior [8] at the lowest energies. Later we will also see this behavior exhibited in the rate coefficients (see Fig. 7) that tend to a constant in the corresponding temperature range. Again referring to Fig. 5, the comparison of the total cross sections of the present work to experimental results [12] shows the best agreement in the energy region above 100 eV/u, but with significant discrepancies for lower energies. The discrepancies are likely related to uncertainties in the incident ion beam and the neutral target. A significant fraction of the incident beam may have included metastable N^+ and doubly charged molecular ions.

The cross sections for charge transfer processes in the collision of atomic nitrogen with H^+ are presented in Fig. 6. We find numerous orbiting resonances in the low energy region for each process. For the collision of $N(2p^3\ ^4S^o)$ with H^+ , comparisons with the calculations of Kimura *et al.* [14] and Cabrera-Trujillo *et al.* [15] illustrate that the theoretical results all

obtained with different methods, are in a good agreement except for the low energy portion of the calculation of Kimura *et al.* In addition, we also display the experimental results of Gilbody *et al.* [13] in Fig. 6, but for collisions of protons with N₂; the concept of additivity appears not to be valid for this collision system, at least for energies less than 1 keV/u. For collisions of metastable N(2p³ 2D^o) with H⁺, we are unaware of experimental or other theoretical data with which to compare our results.

B. Rate Coefficients

In Fig. 7 and Fig. 8, we present the rate coefficients for collisions of N⁺ with atomic hydrogen and H⁺ with atomic nitrogen. The rate coefficients $\alpha(T)$, where T is the temperature, are determined by averaging over the cross section $\sigma(E)$ with the Maxwellian energy distribution,

$$\alpha(T) = \frac{1}{\sqrt{\pi\mu}} \left(\frac{2}{kT} \right)^{3/2} \int_0^{\infty} \sigma(E) E \exp(-E/kT) dE, \quad (5)$$

where k is the Boltzmann constant and μ is the reduced mass of the system.

In Fig. 7, because reaction (1) is endoergic, the rate coefficient drops abruptly to zero as T approaches the threshold. On the contrary, the exoergic reaction (2), tends to a constant. The rate coefficient also displays slight fluctuations due to the orbiting resonances in the cross sections. For reaction (2), the results of Steigman *et al.* [16] are much larger than all other calculations. Comparing our total rate coefficients to the calculations of Butler and Dalgarno [17], we find their results are also larger below 20,000 K, but become smaller than the current results above 20,000 K. The discrepancy is related to the consideration of different coupling mechanisms in the calculations: spin-orbit between the 1 ⁴Σ⁻ and 1 ²Π states in the earlier work and nonadiabatic radial and rotational interactions in the current study. Therefore an estimate of the total rate coefficients can be obtained by summing the results from both mechanisms with spin-orbit coupling dominating below 20,000 K, and radial/ rotational coupling the primary mechanism above 20,000 K.

Rate coefficients for the reverse of reactions (1) and (2) are presented in Fig. 8. For the reverse of reaction (2), our results are smaller than the predictions of Kimura *et al.* and Steigman *et al.* The former discrepancy is consistent with the observation (see Fig. 6) that our cross sections are smaller than those of Kimura *et al.* for energies less than 100 eV/u. The rate coefficients of Kingdon and Ferland [18] were obtained by applying

detailed-balance to the spin-orbit rate coefficients of Butler and Dalgarno. Again they are larger than the current results for temperatures $\lesssim 20,000$ K. A reasonable estimate of the total rate coefficient for the reverse of reaction (1) could be obtained by summing the two results. Finally, no data exists for the metastable nitrogen reaction, the reverse of process (2). The rate coefficient for the process is expected to approach a constant, but apparently for temperatures less than 10 K.

V. ASTROPHYSICAL IMPLICATIONS

Nitrogen is the sixth most cosmically abundant element and as such has been observed in a variety of astrophysical and atmospheric environments. In particular, the role of the charge exchange reaction (2) and its reverse in photoionized gas has been investigated recently. Kingdon and Ferland [19] have studied the role of exothermic charge transfer reactions, such as process (2), on the thermal equilibrium of photoionized nebulae. For a typical model of a nova shell, they found that charge transfer could contribute up to ~ 60 percent of the total heating with most of the contribution coming from reaction (2). Therefore, the magnitude of charge transfer heating is dependent on the value of the rate coefficients for this reaction. In another example, a discrepancy has been known for many years between the observed and predicted emission line ratios of N to N^+ in narrow line region clouds of Seyfert 2 galaxies. Oliva, Marconi, and Moorwood [20] have proposed through extension modeling that if the rate coefficients for reaction (2) and its reverse are reduced by a factor of ~ 30 , then the discrepancy could be resolved. In both cases, the modeling was carried out with the spectral synthesis code Cloudy [21] which incorporates the charge transfer rate coefficients of Butler and Dalgarno [17] for these two processes. Further, the relevant temperatures are between ~ 9000 and 18,000 K. The current rate coefficients, due to radial and rotational coupling, are significantly smaller than the spin-orbit results of Butler and Dalgarno, which were obtained with an approximate spin-orbit coupling value. If this value proves to be overestimated, the discrepancy in the Seyfert 2 galaxy line ratios would be resolved, but the role of charge exchange heating would be reduced. A complete close-coupling calculation involving radial, rotational, and spin-orbit coupling is needed which would be the first of its type that we are aware of. Further, we are unaware of measurements in an energy regime where spin-orbit coupling dominates.

VI. SUMMARY

We have investigated electron capture in collisions of N^+ with H and H^+ with N. Comparison with the existing experimental data suggests that total cross sections from the quantum-mechanical MOCC approach gives reasonable results. The discrepancies at low energy with the measurements of Stebbings *et al.* may be due to considerable experimental uncertainties in the knowledge of the reactant and product species. Further, comparison of the two state-selective cross sections, reveals that $N^+(2p^2\ ^3P^o) + H \rightarrow N(2p^3\ ^4S^o) + H^+$ dominates the total cross section in the low energy regime. However, it becomes nearly equal to capture to the excited state $N(2p^3\ ^2D^o)$ at higher energies. For the collision of N with H^+ , our calculation is very similar to the theoretical results of Cabrera-Trujillo *et al.* and is in good agreement with the calculation of Kimura *et al.* at the highest energies, but not for energies less than 100 eV/u. Total and state-selective measurements are needed for these collision systems.

Rate coefficients given by our calculations are smaller than those reported by Steigman *et al.* and Kimura *et al.* Comparisons with the work of Butler and Dalgarno suggests that radial and rotational couplings is the dominant mechanism for temperatures above 20,000 K, while spin-orbit coupling dominates at lower temperatures.

Acknowledgments

CYL and PCS acknowledge support from NSF grants AST 0087172 and INT 0300708 and NASA grant NAG5-11453. Support is also acknowledged from DF grant Bu 450/7-3 and the Fonds der Chemischen Industrie (RJB & JPG) and the Ministry of ESSCT, JSPS for the US-JP Collaborative Research Program, and a Collaborative Research Grant by NIFS (MK). CYL also acknowledges Libo Zhao for helpful discussions.

-
- [1] P. C. Stancil, B. Zygelman, N. J. Clarke, and D. L. Cooper *J. Phys. B* **30**, 1013 (1997).
 - [2] R. J. Buenker and S. D. Peyerimhoff, *Theor. Chim. Acta* **35**, 33, (1974); **39**, 217, (1975).
 - [3] R. J. Buenker, in *Current Aspects of Quantum Chemistry 1981 (Studies in Physical and Theoretical Chemistry, Vol.21)*, edited by R. Carbo (Elsevier, Amsterdam), p. 17.

- [4] S. Krebs and R. J. Buenker, *J. Chem. Phys.* **103**, 5613, (1995).
- [5] C. Galloy and J. C. Lorquet, *J. Chem. Phys.* **67**, 4672, (1977).
- [6] G. Hirsch, P. J. Bruna, R. J. Buenker, and S. D. Peyerimhoff, *J. Chem. Phys.* **45**, 335, (1980).
- [7] B. Zygelman, D. L. Cooper, M. J. Ford, A. Dalgarno, J. Gerratt, and M. Raimondi, *Phys. Rev. A* **46**, 3846 (1992).
- [8] B. Zygelman, P. C. Stancil, N. J. Clarke, and D. L. Cooper *Phys. Rev. A* **56**, 457 (1997).
- [9] B. R. Johnson, *J. Comput. Phys.* **13**, 445 (1973).
- [10] T. G. Heil, S. Butler, and A. Dalgarno, *Phys. Rev. A* **23**, 1100 (1981).
- [11] N. Shimakura, and M. Kimura, *Phys. Rev. A* **44**, 1659 (1991).
- [12] R. F. Stebbings, W. L. Fite, and D. G. Hummer, *J. Chem. Phys.* **33**, 1226 (1960).
- [13] H. B. Gilbody, and J. B. Hasted, *Proc. R. Soc. London, Ser. A* **238**, 334 (1957).
- [14] M. Kimura, J. P. Gu, G. Hirsch, and R. J. Buenker, *Phys. Rev. A* **55**, 2778 (1997).
- [15] R. Cabrera-Trujillo, Y. Öhrn, E. Deumens, and J. R. Sabin, *Phys. Rev. A* **62**, 052714 (2000).
- [16] G. Steigman, M. W. Werner, and F. M. Geldon, *Astrophys. J.* **168**, 373 (1971).
- [17] S. E. Butler, and A. Dalgarno, *Astrophys. J.* **234**, 765 (1979).
- [18] J. B. Kingdon, and G. J. Ferland, *Astrophys. J. Sup. Ser.* **106**, 205 (1996).
- [19] J. B. Kingdon, and G. J. Ferland, *Astrophys. J.* **516**, L107 (1999).
- [20] E. Oliva, A. Marconi, and A. F. Moorwood, *Astron. Astrophys.* **342**, 87 (1999).
- [21] G. J. Ferland, K. T. Korista, D. A. Verner, J. W. Ferguson, J. B. Kingdon, and E. M. Verner, *Pub. Astron. Soc. Pac.* **110**, 761 (1998).

TABLE I: Comparison of asymptotic separated-atom energies between the MRD-CI calculations and experiments for the eight molecular states of NH^+ . These states are of symmetries $^2, ^4\Sigma^-$, $^2, ^4\Pi$, and $^2\Delta$.

Asymptotic atomic state	Mol. state	This work (eV)	Expt. (eV)
$\text{N}(2p^3\ ^4S^o) + \text{H}^+$	$1\ ^4\Sigma^-$	0.0000	0.0000
$\text{N}^+(2p^2\ ^3P) + \text{H}$	$2\ ^4\Sigma^-$	0.7143	0.9467
	$1\ ^2\Pi$	0.7180	–
	$1\ ^4\Pi$	0.7241	–
	$1\ ^2\Sigma^-$	0.7258	–
$\text{N}(2p^3\ ^2D^o) + \text{H}^+$	$2\ ^2\Pi$	2.6407	2.3840
	$1\ ^2\Delta$	2.6411	–
	$2\ ^2\Sigma^-$	2.6435	–

TABLE II: Rate coefficients for electron capture from collisions of (a): $\text{N}(2p^3 \ ^2D^o)$ and (b): $\text{N}(2p^3 \ ^4S^o)$ with H^+ , and for electron capture into (c): $\text{N}(2p^3 \ ^4S^o)$ and (d): $\text{N}(2p^3 \ ^2D^o)$ from $\text{N}^+(2p^2 \ ^3P) + \text{H}$. (e): total rate coefficients for reactions (c) and (d).

$T(\text{K})$	Rate Coefficients $\alpha(T)$ (cm^3/s)				
	(a)	(b)	(c)	(d)	(e)
6	1.32(-14)		1.08(-14)		1.08(-14)
8	1.73(-14)		1.12(-14)		1.12(-14)
10	2.20(-14)		1.13(-14)		1.13(-14)
20	4.09(-14)		1.09(-14)		1.09(-14)
40	5.82(-14)		9.36(-15)		9.36(-15)
60	7.31(-14)		8.21(-15)		8.21(-15)
80	8.68(-14)		7.42(-15)		7.42(-15)
100	9.60(-14)		6.90(-15)		6.90(-15)
200	1.47(-13)		5.83(-15)		5.83(-15)
400	2.33(-13)		5.64(-15)		5.64(-15)
600	3.20(-13)	1.88(-22)	6.00(-15)		6.00(-15)
800	3.72(-13)	2.05(-20)	6.55(-15)	1.44(-22)	6.55(-15)
1000	4.49(-13)	3.52(-19)	7.19(-15)	1.14(-20)	7.19(-15)
2000	5.89(-13)	1.40(-16)	1.12(-14)	6.13(-17)	1.13(-14)
4000	7.28(-13)	4.91(-15)	2.41(-14)	4.71(-15)	2.89(-14)
6000	8.08(-13)	2.24(-14)	4.31(-14)	2.02(-14)	6.35(-14)
8000	8.87(-13)	5.49(-14)	6.65(-14)	4.43(-14)	1.11(-13)
10000	9.84(-13)	1.06(-13)	9.62(-14)	7.39(-14)	1.70(-13)
20000	1.68(-12)	1.14(-12)	5.64(-13)	2.92(-13)	8.56(-13)
40000	4.64(-12)	1.24(-11)	4.65(-12)	1.31(-12)	5.96(-12)
60000	1.17(-11)	4.00(-11)	1.39(-11)	4.06(-12)	1.80(-11)
80000	2.46(-11)	8.59(-11)	2.87(-11)	9.37(-12)	3.81(-11)
100000	4.33(-11)	1.51(-10)	4.94(-11)	1.73(-11)	6.68(-11)
200000	2.18(-10)	7.50(-10)	2.40(-10)	9.63(-11)	3.37(-10)

The notation $a(-b) = a \times 10^{-b}$

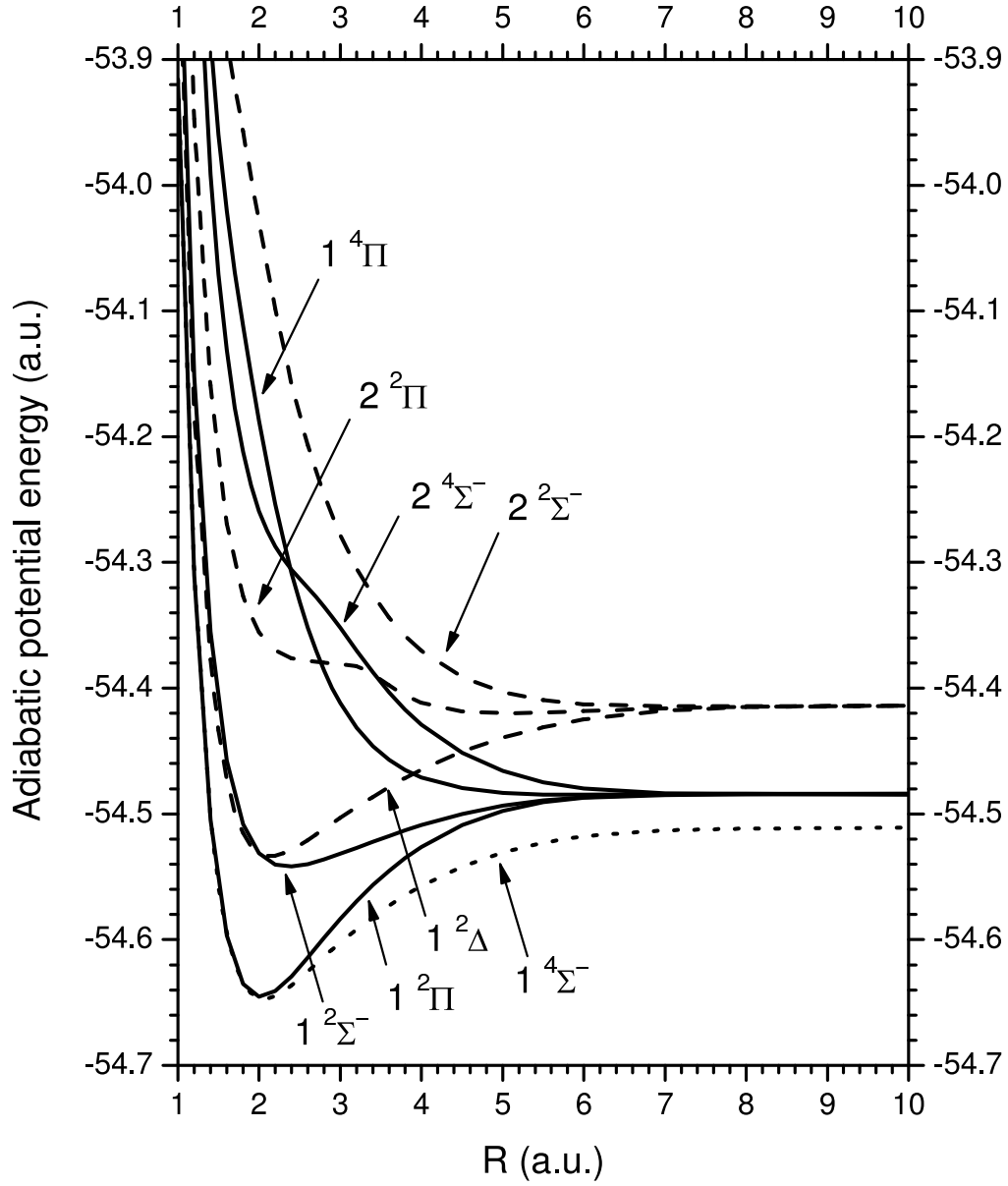


FIG. 1: Adiabatic potentials for NH^+ as a function of internuclear distance R . The dotted curve corresponds to the asymptotic atomic state of $\text{N}(2p^3 4S^0) + \text{H}^+$, solid curves to $\text{N}^+(2p^2 3P) + \text{H}$, and dashed curves to $\text{N}(2p^3 2D^0) + \text{H}^+$.

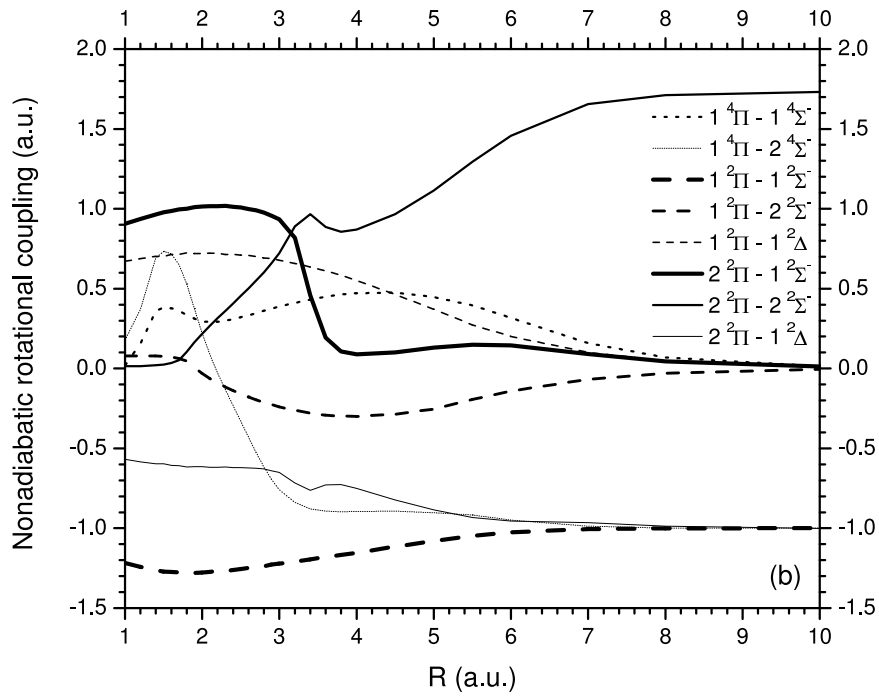
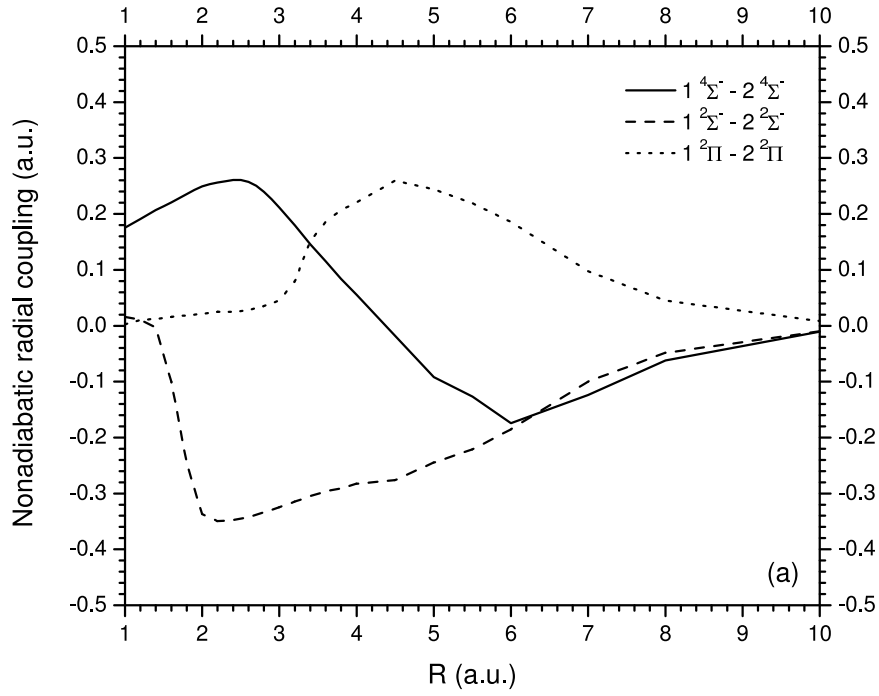


FIG. 2: Nonadiabatic (a) radial and (b) rotational couplings for the NH^+ system as functions of internuclear distance R .

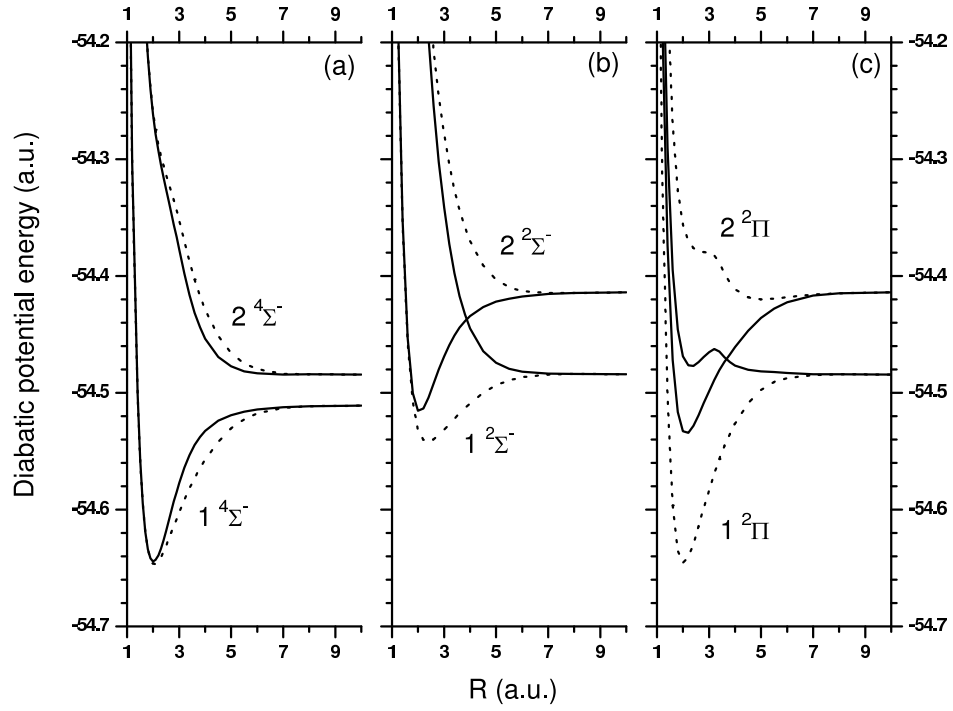


FIG. 3: Diagonal diabatic potential curves (solid lines) compared to the adiabatic potential energies (dotted lines), (a) the quartet Σ^- states, (b) the doublet Σ^- states and (c) the doublet Π states.

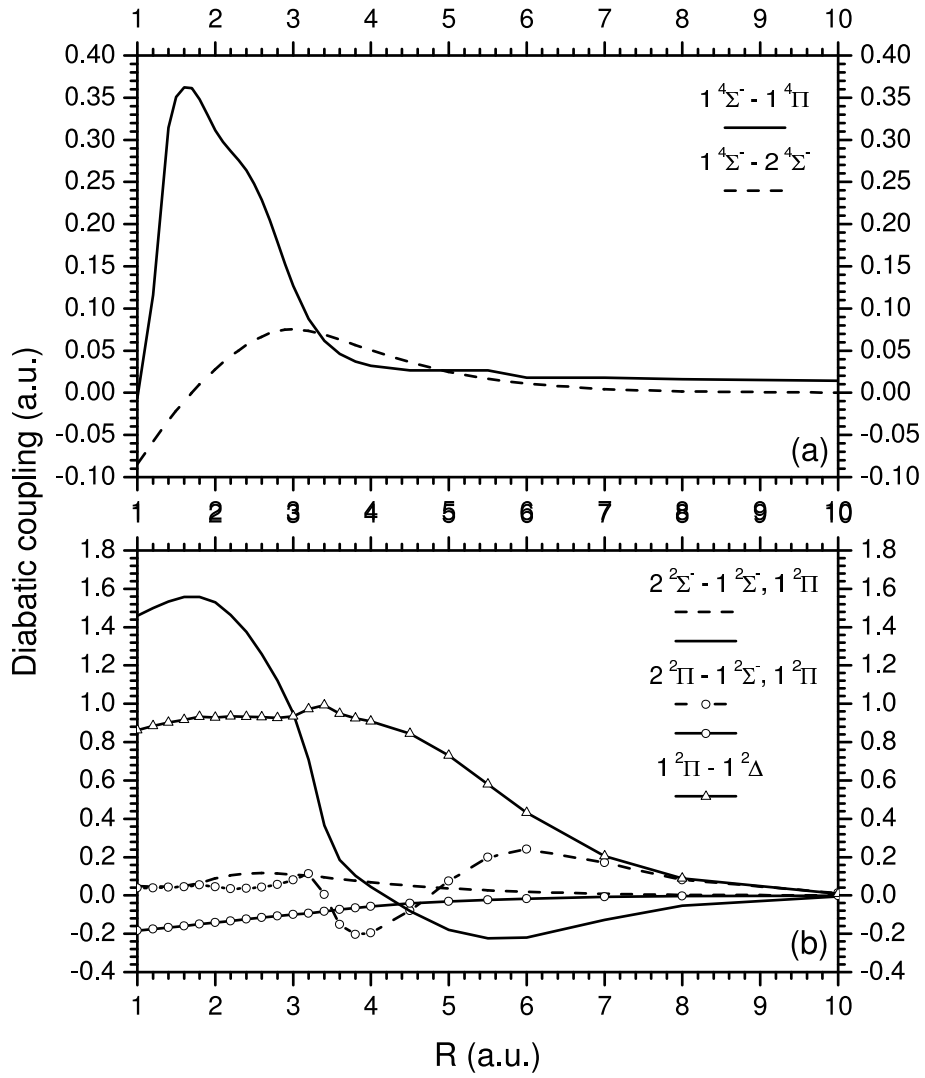


FIG. 4: Off-diagonal diabatic potentials for the (a) quartet, and (b) doublet states of the NH^+ system as a function of internuclear distance R .

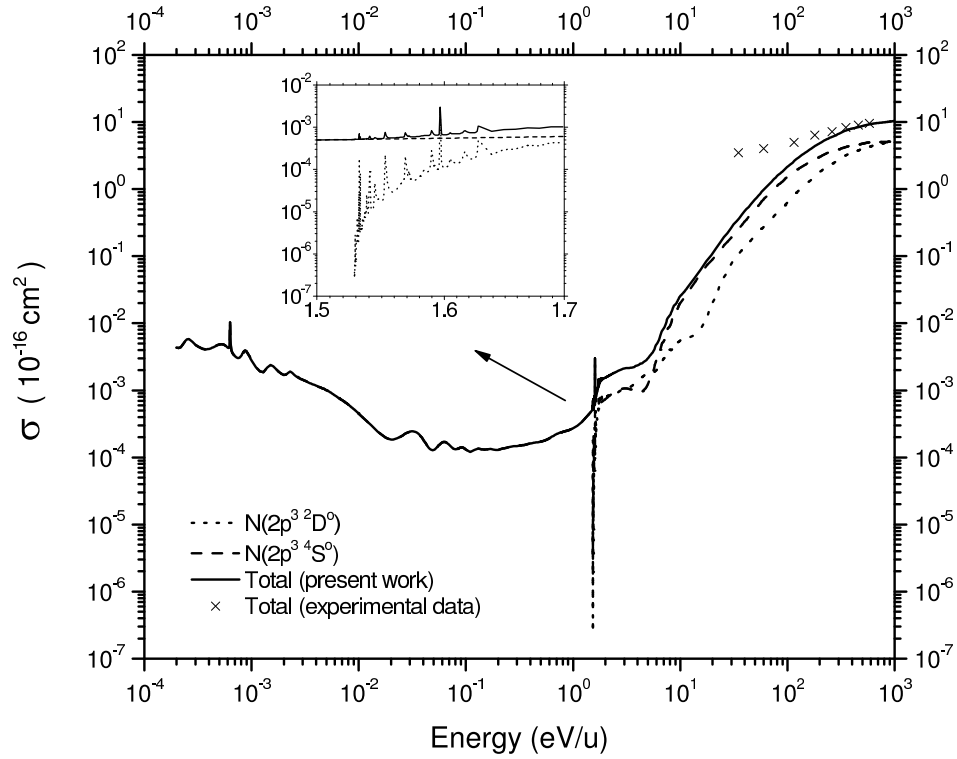


FIG. 5: Total and state-selective electron capture cross sections for $N^+ + H \rightarrow N + H^+$. The dashed and dotted line are state-selective cross sections. The final states of N are indicated in the figure. Solid line and \times are total cross sections for the present work and the measurement of Stebbings *et al.* [12].

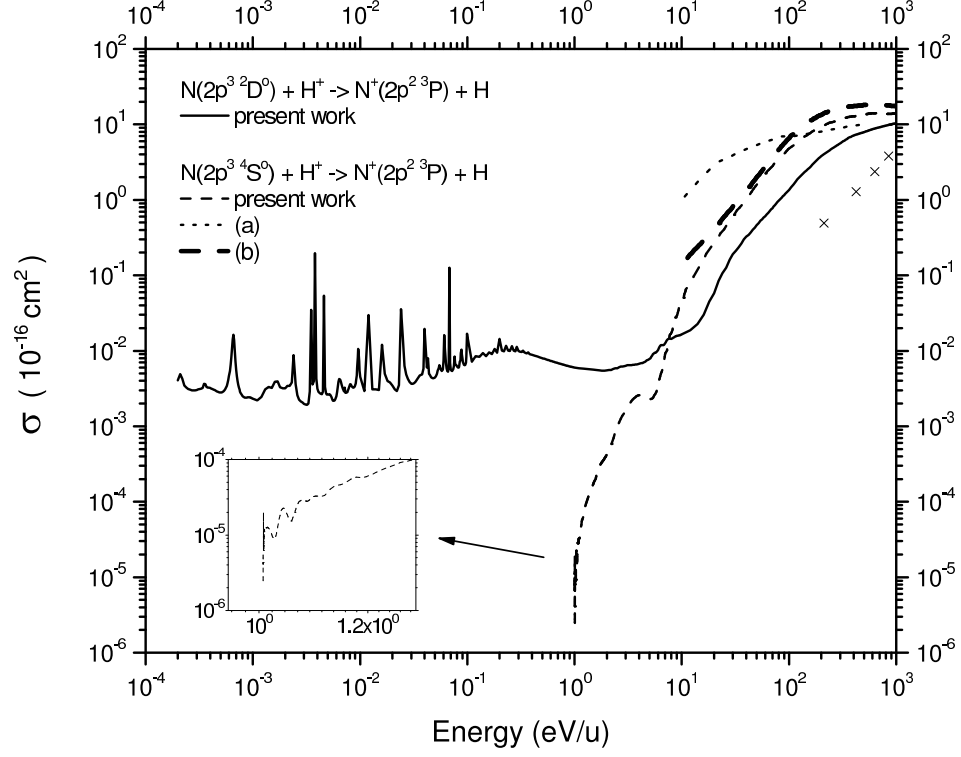


FIG. 6: Total cross sections for $N(2p^3 \ ^2D^o) + H^+ \rightarrow N^+(2p^2 \ ^3P) + H$ (solid line) and $N(2p^3 \ ^4S^o) + H^+ \rightarrow N^+(2p^2 \ ^3P) + H$ (non-solid line: (a) Kimura *et al.* [14] ; (b) Cabrera-Trujillo *et al.* [15]). The experimental values of Gilbody *et al.* [13], indicated by \times , are for proton collisions on N_2 .

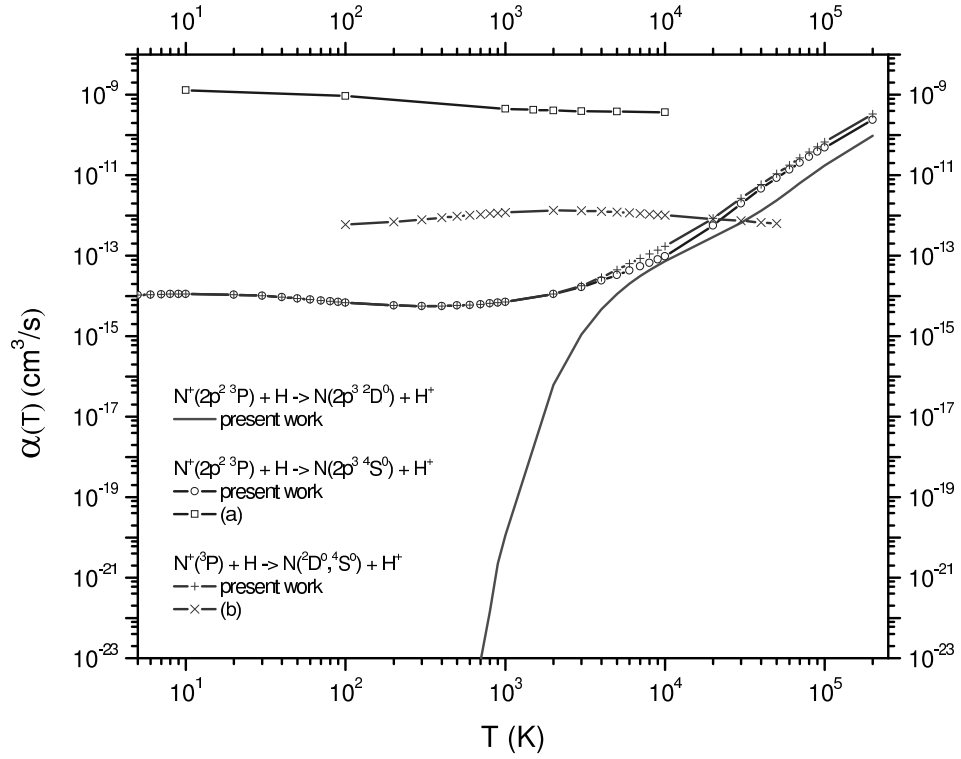


FIG. 7: Rate coefficients for the collision of N^+ with atomic hydrogen as a function of temperature T . (a) and (b) refer to calculations of Steigman *et al.* [16] and Butler and Dalgarno [17] respectively.

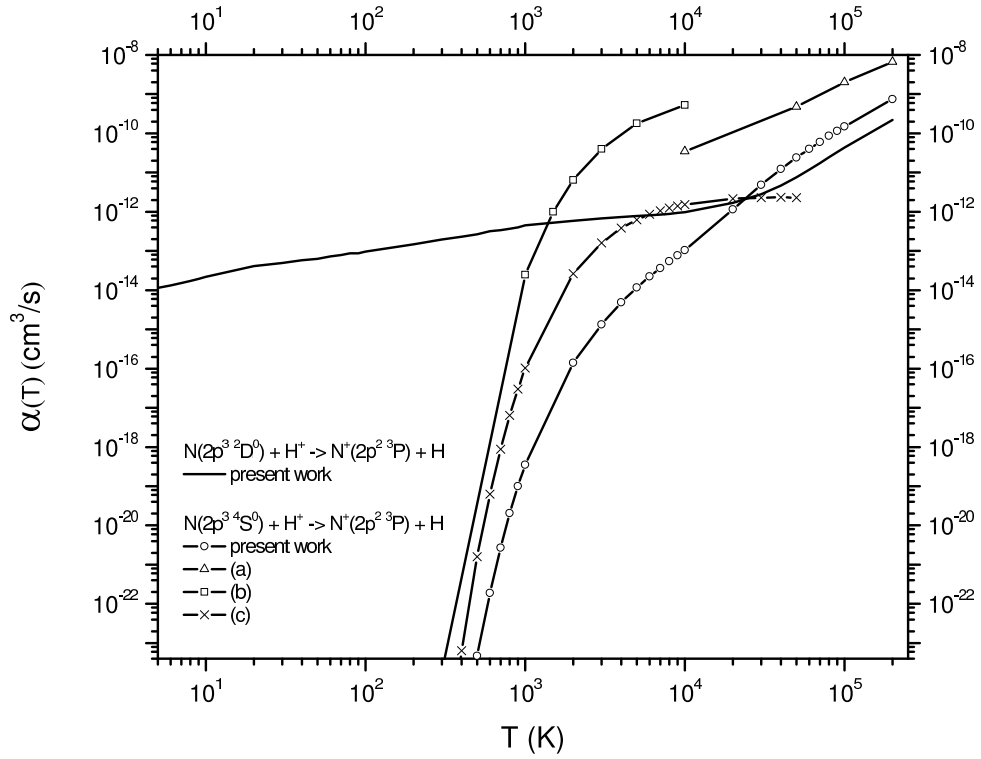


FIG. 8: Rate coefficients for the collision of H^+ with atomic nitrogen as a function of temperature T . (a), (b), and (c) refer to calculations of Kimura *et al.* [14], Steigman *et al.* [16], and Kingdon and Ferland [18] respectively.